



Pergamon

Available online at www.sciencedirect.com

SCIENCE @ DIRECT®

OCEAN
ENGINEERING

Ocean Engineering 30 (2003) 1741–1764

www.elsevier.com/locate/oceaneng

Morphodynamics and cobbles behavior in and near the surf zone

S.I. Voropayev *¹, F.Y. Testik, H.J.S. Fernando, D.L. Boyer

*Environmental Fluid Dynamics Program, Department of Mechanical and Aerospace Engineering,
Arizona State University, Tempe, AZ 85287-9809, USA*

Received 23 August 2002; accepted 11 December 2002

Abstract

The evolution of an initially flat sandy slope and the dynamics of large objects (cobbles/mines) emplaced on it are studied in a laboratory wave tank under simulated surf conditions. Upon initiation of wave forcing, the initially flat beach undergoes bedform changes before reaching a quasi-steady morphology characterized by a system of sand ripples along the slope and a large bar near the break point. Although the incoming wave characteristics are held fixed, the bottom morphology never reaches a strict steady state, but rather slowly changes due to the migration of ripples and bar transformation. When the wave characteristics are changed, the bedform adjusts to a new quasi-steady state after a suitable adjustment time. Studies conducted by placing model cobbles/mines on the evolving sandy bottom subjected to wave forcing show four distinct scenarios: (i) periodic cobble oscillations with zero mean displacement and small scour around the cobbles, (ii) mean onshore motion of relatively light cobbles, (iii) periodic burial of relatively heavy cobbles when their sizes are comparable to those of sand ripples, and (iv) the burial of relatively large cobbles under the bar, when the bar migrates due to changes of incoming waves. Quantitative data on the characteristics and dynamics of the bedform, including ripple-formation front propagating down the slope, ripple growth and drift, and flow around ripples, are presented. Physical explanations are provided for the observations.

© 2003 Elsevier Science Ltd. All rights reserved.

Keywords: Sediment transport; Surf zone; Sand bar and ripples; Cobble and mine dynamics

* Corresponding author. Tel.: +1-480-965-3770; fax: +1-480-965-8746.

E-mail address: s.voropayev@asu.edu (S.I. Voropayev).

¹ Also at the Institute of Oceanology, Russian Academy of Sciences, Moscow, 117851, Russia

1. Introduction

In this communication we present results on the evolution of an initially flat sandy slope and behavior of cobbles placed on it under nonlinear progressive waves in a model surf zone. This research was motivated by the recent naval interests on the behavior and fate of cobble-size objects (mines) in and near the surf zone where nonlinear waves play the dominant role. The fate of disk-shaped cobbles released into the coastal zone is largely determined by the flow surrounding the cobble, the bedform transformation and cobble–sand–flow interaction. This problem has not been studied previously for progressive waves on a sandy slope and the present work constitutes an investigation in this context.

Over the years, extensive research has been conducted on the dynamics of wave motions in the coastal zone and sediment transport therein (Longuet-Higgins and Stewart, 1964; Engelund and Fredsøe, 1982; Peregrine, 1983; Craik, 1985; Battjes, 1988; Yalin, 1977; Mei, 1982; Mei and Liu, 1993; Sleath, 1984; Fredsøe and Deigaard, 1992; Nielsen, 1992; Belorgey et al., 1993; Dean and Dalrymple, 1994; Arcilla et al., 1994; Elfink and Baldock, 2002). Most of these studies have been concentrated on fine sediment transport, and only little attention has been paid to the study of much larger sediment particles, such as cobbles, which are defined by the American Geophysical Union as sediment particles with diameter $D = 6.4\text{--}25.6$ cm (Sleath, 1984). An understanding of the motion of cobble-sized objects has applications in such civil infrastructure problems as coastal protection and safety. Related military applications include the motion and burial of anti-tank mines, the size of which is comparable to cobbles.

Recognizing that the problem of cobble-size mine behavior in the coastal zone has been practically ignored to date, a step-by-step approach from simplified situations to more realistic and complicated configurations was adopted. Initially, experiments were conducted, in which the motion of heavy particles (disks, spheres and spherical shells, filled with liquid to change the moment of inertia) was studied on a solid slope, the background flows used being similar to those observed in different regions of the surf zone (Luccio et al., 1998; Voropayev et al., 1998). Then a layer of sand was placed at the bottom, and the dynamics of sand ripples and effects associated with the scour/burial process of cobbles were studied under oscillatory flow (Voropayev et al., 1999). Later, a large wave tank with a sloping beach was constructed allowing us to model more accurately the main features of water motion in the shoaling region of a surf zone. Experiments were conducted and theoretical models for mine motion, developed previously for simplified flow configurations, were further tested and improved for the case of nonlinear progressive waves on a solid slope (Voropayev et al., 2001). In the present study, the above work is extended to include a homogeneous layer of sand placed on the slope under progressive waves.

The presence of sand significantly complicates the problem. When the fluid velocity exceeds a critical value, ripples are formed on an initially smooth sandy bed; these ripples, in turn, have a strong influence on the sand transport and wave damping in the near shore region. Additionally, these sand ripples can influence the scour/burial of cobbles. The physical mechanism of ripple formation is qualitatively

well understood; see Horikawa and Wanatabe (1967); Sleath (1976, 1984, 1995) and references therein. Owing to the complexity of the sand-ripple problem, however, pertinent quantitative theories are still nascent, and progress in linear and weakly nonlinear analyses for small, the so-called ‘rolling-grain ripples’, have been made only recently (Blondeaux, 1990; Blondeaux et al., 2000; Vittory and Blondeaux, 1990; Andersen, 2001). These features are observed at relatively small amplitudes of the fluid oscillations on initially flat sandy beds. With time, the height of the rolling-grain ripples increases and flow separation becomes possible, forming the so-called ‘vortex ripples’. Analytical theories for kindred nonlinear oscillatory flows are unavailable, and in engineering practice empirical and semi-empirical models are employed for calculations (Sleath, 1984, 1995; Nielsen, 1992).

The behavior of cobble-size objects on a movable bed is dependent on a variety of factors. First, if the fluid velocity is high enough, sand ripples can be formed along the bottom and the slow drift of ripples may lead to periodic burial of cobbles (Voropayev et al., 1999). Additionally, the formation of relatively large sandbars can be expected near the break point (Mei and Liu, 1993; Mei and Yu, 1997). Because relatively light mines move (mostly onshore, Voropayev et al., 2001) along a solid slope in simulated surf, one may expect them to move over the top of the ripples in an onshore direction and subsequently reach the bar. Finally, the most drastic changes of the sandy bottom occur as a consequence of changes in wave characteristics.

Below, in Section 2, experimental set-up and flow conditions are described. Ripple formation and evolution are discussed in Section 3. In Section 4 bar formation and evolution in steady and variable background flows are described. Results on cobble-ripple and cobble-bar interactions are given in Section 5 and the main conclusions are summarized in Section 6.

2. Experimental set-up and flow conditions

2.1. Experimental set-up

A detailed description of the experimental facility can be found in Voropayev et al. (2001, 2003) and only a brief description is given below. A large glass-walled wave tank ($32 \times 0.9 \times 1.8$ m) with a slopping bottom is used in experiments to generate progressive waves. The tank is filled with tap water (density $\rho = 1 \text{ g cm}^{-3}$, viscosity $\nu = 10^{-2} \text{ cm}^2 \text{ s}^{-1}$) to a depth of $H_0 = 100$ cm near the wave paddle where the tank bottom is horizontal (see schematic in Fig. 1). The tank consists of a number of sections, which are numbered 0 to 47, with section 0 being the panel to the left of the wave maker and each section is 61 cm in length. For convenience, the section numbers will be referred to indicate the horizontal position along the slope. A vertical paddle, driven by a piston installed at one end of the tank, is used to generate sinusoidal periodic waves of frequencies $\omega = 2\pi(0.4\text{--}0.75 \text{ Hz}) \text{ rads}^{-1}$ (in all formulas below ω in rads^{-1} is used) and peak-to-peak displacement of the paddle motion of $2\epsilon_0 = 10\text{--}25$ cm. A layer of quartz sand (mean grain size $d =$

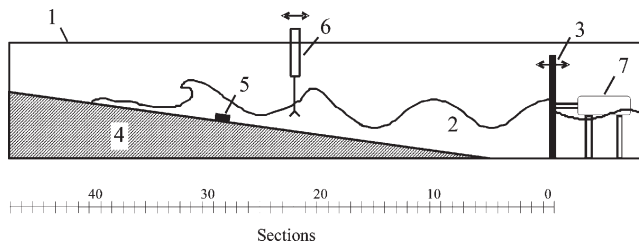


Fig. 1. A schematic diagram of the experimental setup: 1, tank; 2, water; 3, vertical wave-maker (frequency ω , amplitude of horizontal displacement ϵ_0), 4, sloping sand bottom; 5, cobble; 6, acoustic Doppler velocimeter (ADV) attached to carriage; 7, hydraulic system to move the wave maker. Section numbers are also shown and the length of one section is 61 cm.

0.06 cm, density $\rho_s = 2.6 \text{ gcm}^{-3}$) of thickness 20 cm was placed on the wooden bottom with a slope of 1:24 (length 26 m). To monitor the flow characteristics, the wave elevations and the horizontal and vertical velocity components were measured at different locations (sections) along the slope using standard wave gages and a three-component acoustic Doppler velocimeter (ADV) (Snyder and Castro, 1999). The ADV probe, which is attached to a long supporting rod, is fixed to a carriage that is mounted on rails on top of the tank. To obtain representative data, the velocity records were phase averaged for a time interval of 40 oscillation periods. The carriage has three degrees of freedom, movement along the tank, as well as transverse and vertical directions.

Before each experiment the sand on the slope was leveled and made flat. Three series of experiments were conducted. In the first series, flow characteristics of progressive waves propagating and breaking along the sandy slope were documented in the absence of cobbles. In the second series, the time evolution of an initially flat sandy slope (the formation of ripples and bar, and growth and drift of ripples) was documented. A cobble was then placed on the fully developed sandy slope (with ripples and bar) and its behavior was investigated.

Information on the bottom topography and the behavior of the cobble was obtained using Super VHS video cameras. For selected cases, photographs were also taken using a standard 35-mm still camera. After the experiment, video records were analyzed and data on topography changes and cobbles behavior were obtained.

2.2. Cobbles

The experiments were performed with a variety of cobbles, all disk-shaped but with different size (diameter D and height H_C) and density (ρ_C) (see Table 1). Cobbles 2 and 3 are replicas of anti-tank mines. They are made of plastic, but have size and weight ranges that are compatible with real mines.

2.3. Background flow characteristics and their parameterization

Although the wave-maker forcing is purely sinusoidal, as they propagate along the slope the waves steepen, change the height and underlying velocity profile become

Table 1
Cobbles/mines characteristics

No.	Diameter D (cm)	Height H _c (cm)	Mass (kg)	Density ρ _c (g cm ⁻³)
1	20.0	8.4	3.02	1.18
2	21.8	9.3	2.94	1.08
3	21.3	9.3	3.36	1.29
D	10.2	4.4	0.55	1.62
E	7.6	3.5	0.21	1.50
F	9.1	2.4	0.21	1.40
G	7.5	2.4	0.13	1.18

nonlinear. A typical nonlinear wave propagating (Fig. 2a) from right to left along the sandy slope and then breaking (Fig. 2b) near the break point is shown in Fig. 2. Since the information on the water motion is imperative for the interpretation of observations, the wave elevations and velocities under the waves were measured using a wave gauge and an ADV. These data were taken at different sections (with sampling frequency 24 Hz) along the slope after the flow was established and then were averaged over 40 oscillation periods.

Typical time records for the horizontal (along slope) velocity component, u , at four different sections along the slope are shown in Fig. 3 (however, data were taken at each section between 13 and 31). By integrating these velocity records over time, the amplitude of the water particle displacement, ϵ , can be calculated. Note that the water motion varies significantly with the position along the slope. This variability complicates the interpretation of data on bottom morphodynamics (in particular ripple formation and migration, see below) under surf conditions. Kindred data were obtained for different experimental conditions (ω , ϵ_0 and measurement depth above the bottom), providing information on the corresponding maximum velocity amplitude, U , and wave height, η^* , along the slope.

Usually the experiments on sandy bed morphodynamics under waves are interpreted using the mobility, Ψ , or Shields, Sh , parameter and dimensionless time, τ , which are defined as

$$\Psi = U^2/g*d, \quad Sh = U^{*2}/g*d = U(v\omega)^{1/2}/g(s-1)d, \quad \tau = \omega t. \quad (1)$$

Here U is the maximum horizontal water velocity in the area of interest, g the gravitational acceleration, $g^* = g(s-1)$, $s = \rho_s/\rho$, $U^* = U(f/2)^{1/2}$ the friction velocity, $f = 2^{3/2}/Re_0$ the friction coefficient, $Re_0 = \delta U / = 2^{1/2}U/(v\omega)^{1/2}$ the boundary layer Reynolds number and $\delta = (2\nu/\omega)^{1/2}$ the boundary-layer thickness (Sleath, 1984; Nielsen, 1992).

For waves on a horizontal bottom, the values of Ψ and Sh do not depend on the horizontal distance, x , along the bed. This is the case for progressive waves on a sloping beach, as U increases with decreasing water depth, H . At present no formal theories are available to predict accurately such nonlinear behavior, and the predictions need to be based on sophisticated numerical simulations (see, for example, Grilli and Horillo, 1997; Grilli et al., 1997). These simulations, however, require

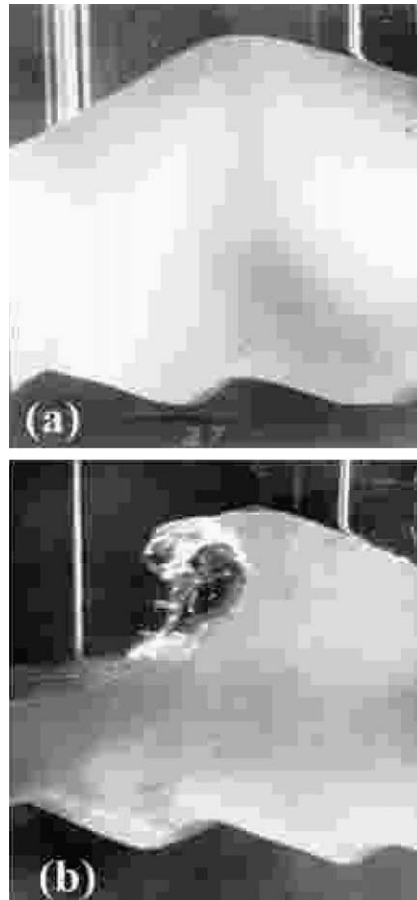


Fig. 2. A typical nonlinear wave propagating (a) from right to left along sandy slope and then breaking (b) near the break point. Experimental parameters: $\omega = 0.4$ Hz, $\epsilon_0 = 10$ cm, section 27 (a), 29 (b). Sand ripples are clearly seen at the bottom.

detailed verifications using experimental data (see Grilli et al., 2003). For simplicity, in the present study we adopted a simple approach to calculate local wave properties in support of the interpretation of results. This approach is described below.

The paddle velocity, U_p , changes sinusoidally with frequency ω and amplitude ϵ_0 ,

$$U_p = U_0 \sin \omega t = \epsilon_0 \omega \sin \omega t, \quad (2)$$

generating waves of constant frequency ω that propagate onshore while increasing their height, η , and decreasing the wavelength, λ . Offshore of the breaking point, the energy dissipation in waves approaching the beach is negligible and the flux of energy Φ in the direction of wave propagation can be assumed to be constant (Sleath, 1984); i.e.,

$$\Phi = c_g \rho g \eta^2 / 8 = \text{const.} \quad (3)$$

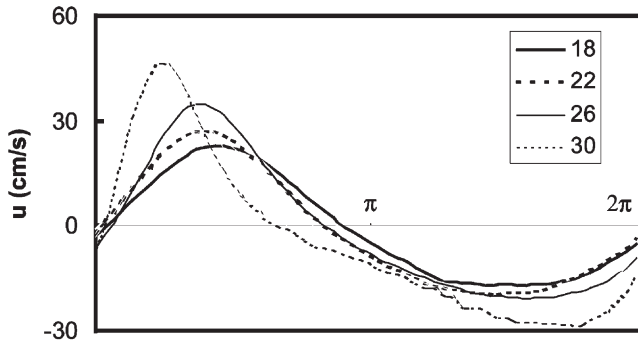


Fig. 3. Horizontal along-slope water velocity, u , for different distances (sections) along the slope. The data were taken in different sections (see insert) and phase averaged over 40 wave periods. The depth of measurements is 10 cm above the bottom. Experimental parameters: $\omega = 0.4$ Hz, $\epsilon_0 = 5$ cm. For clarity, only four velocity profiles are shown.

In shallow water the group velocity $c_g = c$, and the wave celerity is given by

$$c = \omega/k = (gH)^{1/2}, \tag{4}$$

where $k = 2\pi/\lambda$ is the wave number and H is the mean local water depth, which depends on the position, x , along the slope and the slope angle, β as

$$H = H_0 - x \tan\beta, \tag{5}$$

where H_0 is the water depth near the paddle. The wave height, η_0 , and length, λ_0 , near the pedal can be estimated as (Dean and Dalrymple, 1994)

$$\eta_0 = 2\pi\epsilon_0 H_0/\lambda_0, \quad \lambda_0 = (gH_0)^{1/2} 2\pi/\omega. \tag{6}$$

Using (3), (4), (6), it is possible to estimate

$$\eta = \eta_0(H_0/H)^{1/4} = \epsilon_0\omega H_0^{3/4}/g^{1/2}H^{1/4}, \tag{7}$$

where H is given in (5).

Water particles under waves make ellipsoidal trajectories, and the amplitude of the horizontal particle excursion in shallow water can be estimated as (Dean and Dalrymple, 1994)

$$\epsilon = \eta/kH = \eta g^{1/2}/\omega H^{1/2} \tag{8}$$

where (4) was used. From (6)–(8), we obtain

$$\epsilon = \epsilon_0(H_0/H)^{3/4}, \quad U = \epsilon\omega = U_0(H_0/H)^{3/4}. \tag{9}$$

The measured values of U along the slope are shown by symbols in Fig. 4 and solid line shows the estimate (9); the agreement is satisfactory. The local values of Ψ and Sh along the slope for different ω and ϵ_0 were calculated using (9). The other parameters, H_0 , β , d and ρ_s , were held fixed in the experiments.

To estimate the wave breaking position, x^* , the criterion proposed by Miche in 1944 (see Sleath, 1984) for progressive waves can be used: $\eta^*k/\pi = 0.142$

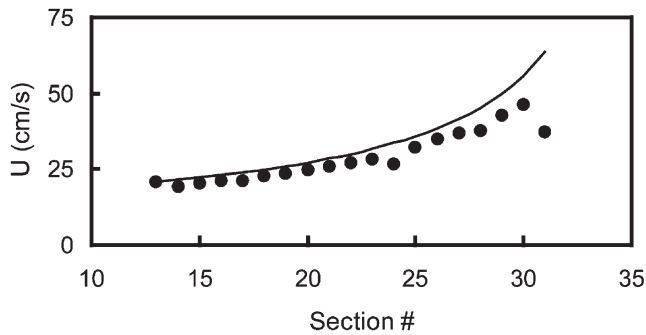


Fig. 4. A typical distribution of the maximum water velocity, U , along the slope. Symbols show the measured values and the solid line shows the estimate given by (9). Experimental parameters: $\omega = 0.4$ Hz, $\epsilon_0 = 5$ cm.

$\tanh(H^*k)$, where η^* and H^* are the wave amplitude and still water depth near the break. The shallow water assumption simplifies the above formula, and the use of (5) and (7) gives simple estimates

$$H^* = 1.9[\epsilon_0\omega H_0^{3/4}/g^{1/2}]^{4/5}, \quad x^* = (H_0 - H^*)/\text{tg}\beta. \quad (10)$$

3. Sand ripples on a slope

3.1. Qualitative description of ripple formation and evolution

In these experiments, first the sandy slope was made flat (Fig. 5a). Then the waves were generated and the time evolution of the bedform was observed in the absence of cobbles. Qualitatively the observations can be described as follows. After the waves are generated, an oscillatory shear stress is developed near the bottom. If the local Shields parameter exceeds a critical value Sh^* (≈ 0.05 , Sleath, 1984), ripples start forming on the bed. First, relatively small (typical height 0.5 cm) 3D rolling grain ripples are formed. With time, their height increase, they merge, forming the well-known 2D vortex ripples oriented across the flow (Fig. 5b). These 2D ripples initially have a relatively small height, h , and spacing, L , but with time their size increases and, after typical adjustment time interval, $2t^*$ (this time is defined in Section 3.2 below), they reach a quasi-steady equilibrium state (Fig. 5c) with a characteristic (mean over a number of ripples) height, h_0 , and spacing, L_0 . Note that the ripple formation does not occur uniformly along the slope (Fig. 6). At early times, ripples are generated rapidly just offshore of the breaking point where the velocity amplitude (and the mobility or Shields parameter) has a maximum value. Then the ripple-formation zone propagates (see Fig. 6b,c) as a front in the offshore direction (down-slope) and after some time, the slope is either completely or partially covered with ripples depending on the experimental parameters. The front propa-

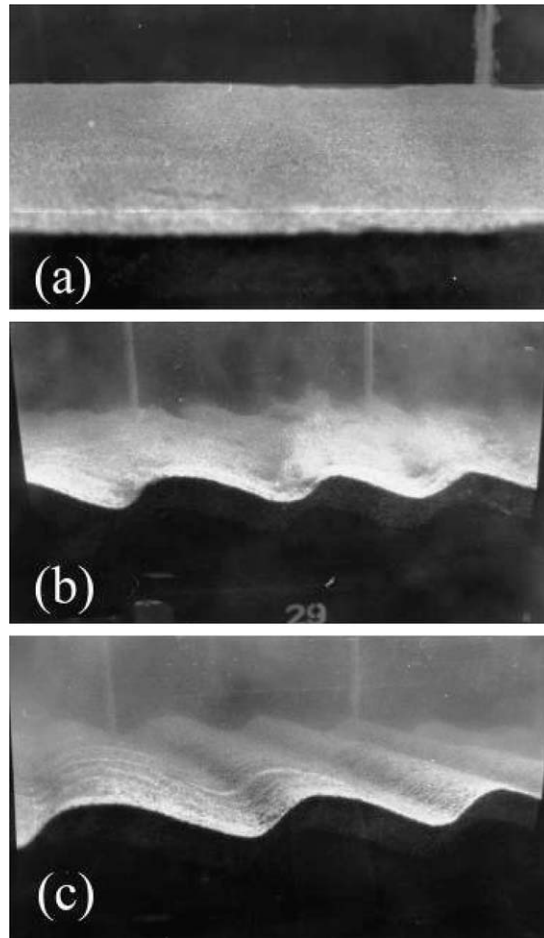


Fig. 5. Side view photographs showing: initially flat sandy bottom (a), growing (b) and quasi-steady (c) 2D sand ripples formed on a slope under progressive waves with relatively large intensity after approximately 3 (b) and 6 (c) min. Experimental parameters: $\omega = 0.4$ Hz, $\epsilon_0 = 8.5$ cm, section 29. The horizontal size of frames (61 cm) gives a length scale.

gation velocity depends strongly on the position along the slope and decreases with the increasing distance from the break point.

The characteristics of the established quasi-steady 2D ripples depend on the position along the slope and ripple size decreases in the offshore direction from the break point. At large times, $t \gg t^*$, the morphology of the ripple bed continues to change and ripples demonstrate large time instabilities and drift slowly in the onshore direction.

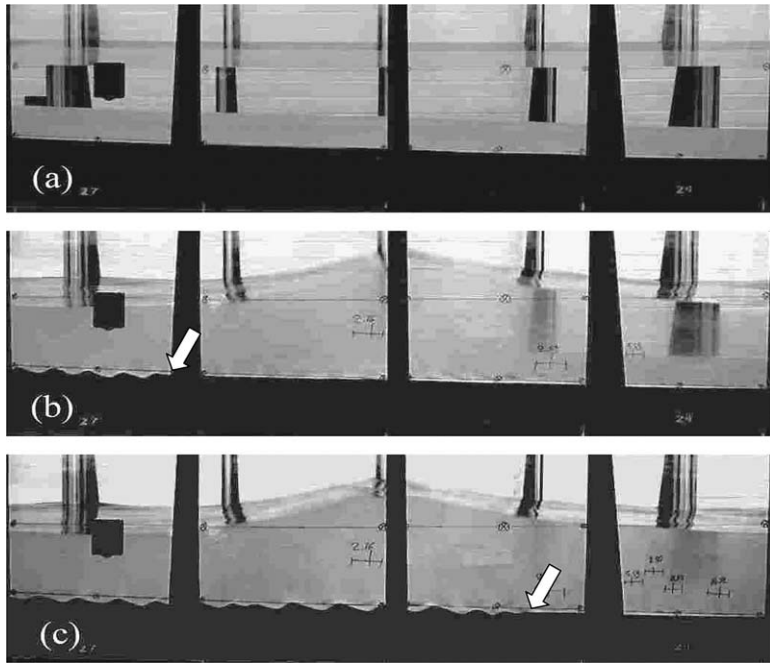


Fig. 6. Ripple front (shown by arrow) propagating (b, c) along initially flat slope (a) in the offshore (from left to right) direction. Parameters: $\omega = 0.4$ Hz, $\epsilon_0 = 7.5$ cm, $t = 0$ (a), 3 (b), 10 min (c).

3.2. Data and interpretation

Before discussing the results of measurements, we will first make some useful estimates. In Voropayev et al. (1999), it was shown that for the case of spatially homogeneous flow on a horizontal bed, the non-dimensional length, L/L_0 , and height, h/h_0 , of ripples increase with the non-dimensional time, t/t^* , as

$$L/L_0 = 1 - \exp(-t/t^*), \quad h/h_0 = 1 - \exp(t/t^*), \tag{11}$$

where L_0 and h_0 are equilibrium ripple length and height, respectively, and

$$t^* = C/\omega\Psi^{1/2}, \tag{12}$$

is a characteristic time scale for ripple formation on initially flat bottom, $C = 2500$ is an empirical constant and Ψ is given in (1). For the spatially homogeneous periodic flow used by Voropayev et al. (1999), the measured values of L_0 and h_0 agreed well with the well-known semi-empirical formulae (Sleath, 1984; Nielsen, 1992)

$$L_0 = \epsilon(2.2 - 0.35\Psi^{1/3}), \quad h_0 = L_0(0.18 - 0.24Sh^{3/2}). \tag{13}$$

In modifying (13) for progressive waves on a sloping beach, one should take into account that ϵ , Ψ and Sh are no longer constant, but change along the slope. To the

first approximation, such changes can be accounted using (1), (5) and (9). These relations were used below to calculate local values of Ψ , Sh and t^* , and then L_0 and h_0 in (13) for different positions (sections) along the slope.

Data for L and h as functions of time t were taken along the slope for different incoming wave characteristics, and they are shown in Fig. 7 in non-dimensional form. Solid lines in this figure represents (11). It appears that parameterizations in (11) are robust, and representative for measurements taken under different conditions. Note that the typical time, at which the system reaches the equilibrium state, can be defined as $2t^*$ (time for $L \approx 0.86 L_0$). This estimate gives not only the characteristic time scale of ripple formation on an initially flat sloping/horizontal bottom, but also the typical time of ripple adjustment due to changes of background conditions (e.g. changes of wave parameters). The simple modification (11) that accounts for the bed

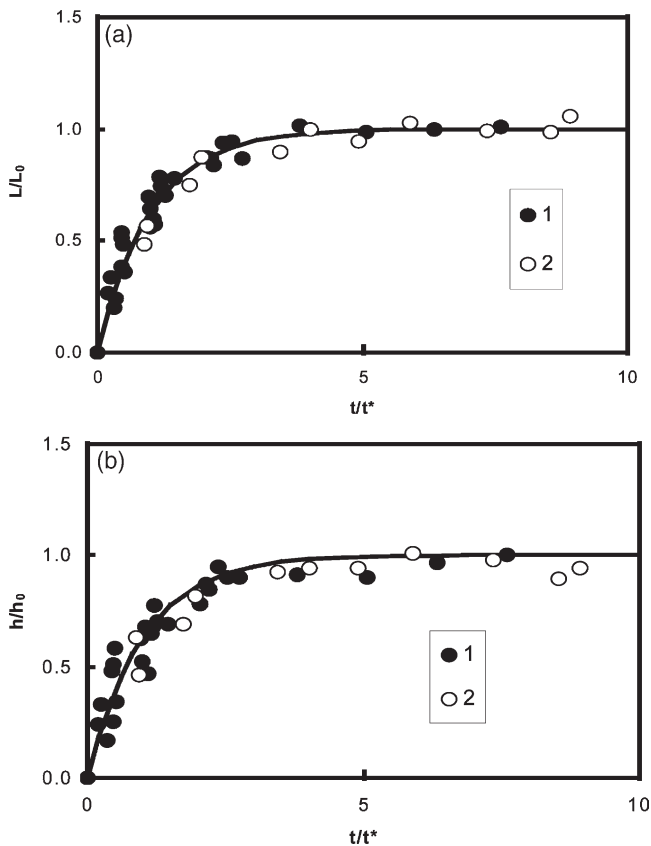


Fig. 7. The non-dimensional ripple length, L/L_0 (a), and height, h/h_0 (b), as functions of the non-dimensional time, t/t^* , for ripples formed at different positions on a slope. Experimental parameters: $\omega = 0.4$ Hz, $\epsilon_0 = 10$ cm (1), 0.75, 6 (2). The data were taken in sections 9/10, 12/13, 16/17, 0/21, 26/27 (1) and 20/21, 26/27, 28/29 (2). Solid lines show the approximation function (11).

slope collapses the experimental data to a single curve with a standard deviation of approximately 15%.

As mentioned earlier, on a slope, ripples start forming first close to the breaking point. Here the flow velocity (and mobility parameter) has a maximum and the characteristic time, t^* , necessary for the ripple formation is a minimum. This leads to a ripple front that propagates with decreasing velocity down the slope into the deep water (see Fig. 6). If the waves are not very energetic, than after some typical time, t_0 , the ripple front stops propagating along the slope at a distance, S_0 , from the point of ripple formation near the break point. As a result, part of the slope is covered with ripples while the rest remains flat for a long time (4–5 h). For very energetic waves, S_0 is rather large and ripple front propagates along the entire slope.

In selected runs, S , and its maximum value, S_0 , were measured and the results are shown in Fig. 8 in a non-dimensional form using S_0 and a typical time t_0 as length and time scales, similar to that in Fig. 7. Assuming that the dynamics here is typical of relaxation processes following perturbations caused by internal or external forcing, we may suppose that the rate of change of S (ripple front propagation speed) decreases exponentially with time, t . This gives an estimate similar to (11)

$$S/S_0 = 1 - \exp(-t/t_0), \tag{14}$$

where $t_0 = t^*$ (at $\Psi = \Psi_0$) = C_0/ω , Ψ_0 (≈ 4) is a critical value of the mobility parameter below which ripples stop forming, $C_0 = C/\Psi_0^{1/2}$ and t^* is given in (12). The best fit gives $C_0 = 1100$ and the estimate (14) is shown by a solid line in Fig. 8, which shows a satisfactory agreement with the data. Unfortunately, we were not

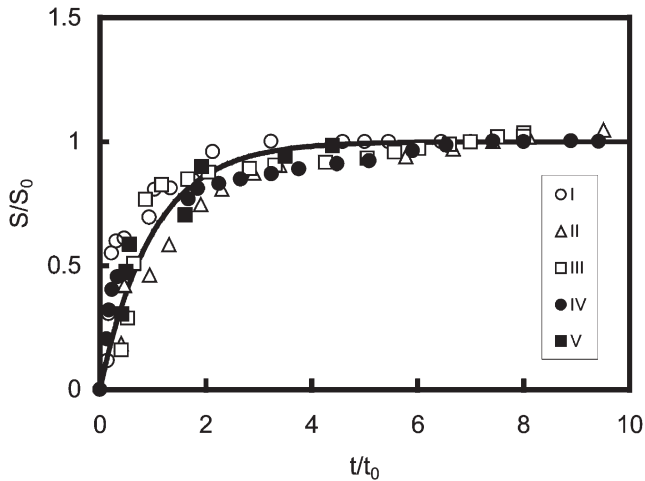


Fig. 8. The non-dimensional ripple front distances, S/S_0 , as function of the non-dimensional time, t/t_0 , for ripple front propagating down the slope. Experimental parameters: $\omega = 0.4$ Hz, $\epsilon_0 = 7.5$ cm (I), 0.75, 5 (II), 0.75, 7.5 (III), 0.4, 7.5 (IV), 0.4, 5 (V). To show the scatter of the experimental data, two experiments (I and IV) were conducted at the same conditions. Solid line shows (14). The measured values of S_0 and the breaker type are as follows: 510 cm, plunging (I), 380, spilling (II), 470, spilling (III), 410, plunging (IV), 130, plunging (V).

able to find a satisfactory parameterization for S_0 (its typical values are given in caption to Fig. 8). While the position of first ripple front appearance can be estimated satisfactorily using (10), the position where the front stops (and thus S_0) was difficult to estimate on physical grounds. For example, the use of some critical value of mobility or Shields parameter to estimate the position where the ripple front stops, gives correct qualitative trend, but quantitatively overestimates S_0 , sometimes by a factor two.

At large times, $t \gg t^*$, the morphology of the rippled bed continues to change, although the mean ripple characteristics L_0 and h_0 (at a fixed position along the slope) do not change appreciably after the formation period $2t^*$; i.e. the bottom topography never reaches an exact steady state. While the frequency and amplitude of the paddle oscillations remain constant, the ripples generated on the bed demonstrate large time instabilities and slow onshore drift.

The first type of instability is related to the periodic merger and split of ripples. This effect was observed and explained for the case of a horizontal sandy bottom under spatially homogeneous oscillatory flow by Voropayev et al. (1999). This process resembles the appearance of periodic dislocations in an initially regular ripple pattern. The dislocation induces migration of ripples in the proximity, and with time the new or merged ripples spread across the flow. Because the typical spacing between ripples decreases/increases during ripple merging/splitting, the whole system of ripples migrates with some typical ‘stochastic’ drift velocity U_{d*} . With time, a new quasi-steady state with approximately the same typical spacing, L_0 , between ripples and height, h_0 , is established. In spatially homogeneous oscillatory flow, the migration velocity has no preferred direction and the mean drift velocity as averaged over large time tends to be zero. The typical absolute value of this velocity for ripples over a horizontal bottom may be estimated as (Voropayev et al., 1999)

$$U_{d*} = L_0/8t^* = U\Psi^{1/2}(2.2 - 0.35\Psi^{1/3})/8C. \quad (15)$$

The observations collected in the present study show that, in addition to the above-mentioned instability, another type of instability is possible under progressive waves on sloping beaches. This instability causes a steady onshore ripple drift with unidirectional drift velocity, U_d , along the slope.

In the present experiments, the net drift velocity, U_d , of ripples was determined by periodically measuring the mean (averaged over one section) displacements of ripple crests over a given period of time, typically 3–5 min. These data were averaged over a longer period of time, typically $(2-3)t^* \approx 15-30$ min, and the mean values of U_d for each section were obtained. Since the mean (over large time) value of the ‘stochastic’ component U_{d*} should be zero, the resulting net migration velocity U_d is equal to the mean unidirectional drift velocity. Note, however, that for representative averaging inside one section, the averaging time should not exceed the time needed for ripples to drift one section length, 61 cm, and if U_{d*} is comparable with U_d , this restriction may lead to significant scatter in the measured values of U_d . Before presenting the results of the measurements, let us first attempt some simple estimates for U_d for which there are no analytical predictions available hitherto.

Kennedy (1963) and Engelung (1970) considered a model for sediment transport

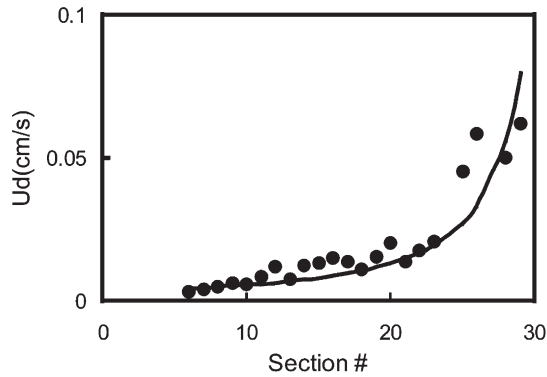


Fig. 9. Ripple drift velocity, U_d , as a function of the along slope position. Symbols show measured values for an experiment with $\omega = 0.4$ Hz, $\epsilon_0 = 10$ cm, solid line shows the estimation based on (18).

resulting from unidirectional drift of sinusoidal bedform with constant shape. From their model, it follows (see also Nielsen, 1992, p. 133) that the drift velocity U_d of such bedform is related to the (volume) sediment flux Q as

$$U_d = Q/nh_0, \tag{16}$$

where n is the volume of solid fraction in a unit volume of the bed (for sand, $n \approx 0.7$), h_0 the bedform height (established ripple height in our case) and the sign of U_d depends on the sign of Q . When the sediment transport rate over the crest is at a maximum, the bedform moves downstream (onshore in our case). In our experiments, unidirectional ripple drift was mostly observed during the forward wave half-cycle wherein maximum sediment transport occurs over the crests (see Fig. 13a below). Using the following empirical expression for Q in (16) for the mean transport during the forward half-cycle of waves (Sleath, 1984, p. 278)

$$Q = \omega d^2(\Psi/10)^{3/2}, \tag{17}$$

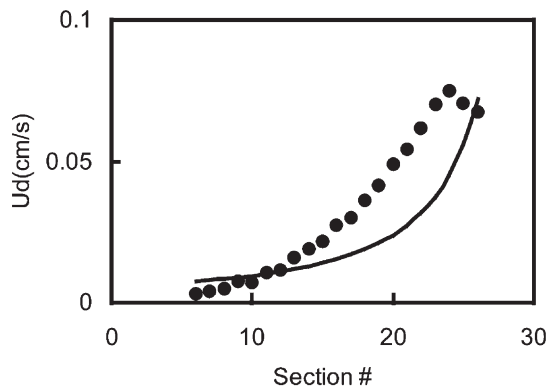


Fig. 10. Same as in Fig. 9 but for $\omega = 0.4$ Hz, $\epsilon_0 = 12.5$ cm.

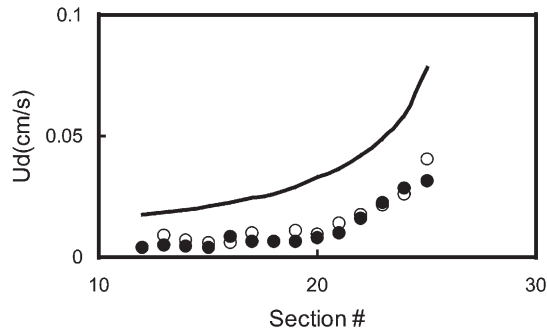


Fig. 11. Same as in Fig. 9 for two experiments (different symbols) with the same parameters: $\omega = 0.6$ Hz, $\epsilon_0 = 7.5$ cm.

it is possible to obtain the estimate

$$U_d = \omega d^2 (\Psi / 10)^{3/2} / nh_0. \quad (18)$$

The data on U_d were collected for different along slope positions (section number), and typical results for two experiments are shown in Figs. 9 and 10. The estimates based on (18) (where local values of ϵ and U in (9) are used to calculate local Ψ and Sh in (1) and h_0 in (13)) are shown by solid lines. For both cases, the drift velocity, U_d , is positive (in the onshore direction) and increases along the slope reaching a maximum near the break. Although there are some differences between the measured and estimated values for U_d , the general agreement is satisfactory. Much poorer agreement was observed, however, at smaller transport rates (where (16) is not very accurate, see Sleath, 1984). In this case (Fig. 11), (18) overestimates U_d by a factor of two. In Fig. 11, the data for two identical experiments are presented to illustrate the measurement errors.

To gain a better understanding of sediment transport and ripple drift, it is useful to investigate the flow around ripples. Recently, Ridler and Sleath (2000) reported observations on the Eulerian time-mean drift induced by waves over solid artificial ripples placed at the bottom of a water layer of constant depth. In their work, velocity measurements were taken at different distances from a crest and a trough and then phase averaged. A mean negative (offshore) water drift was observed near the bed over ripple troughs. Just above the ripple crests in the boundary layer, however, a positive (onshore) mean water drift was documented. No similar data exist for naturally formed (moving) sand ripples, and hence an attempt was made to obtain such measurements. Owing to the drift and spatial variability of sand ripples, however these measurements are more intricate and some results are described below.

The ADV probe was placed in the middle of the tank in section 27 (Fig. 12). In addition to the velocity, the ADV probe can measure the distance to the bottom (by measuring the time interval between the emitted and reflected sound signals) with an accuracy ≤ 0.1 cm. Using this latter capability, measurements of the ripple profile were taken every 10 s while ripples are drifting onshore under the stationary probe (Fig. 12). Using these data and measuring the ripple length, the averaged ripple drift

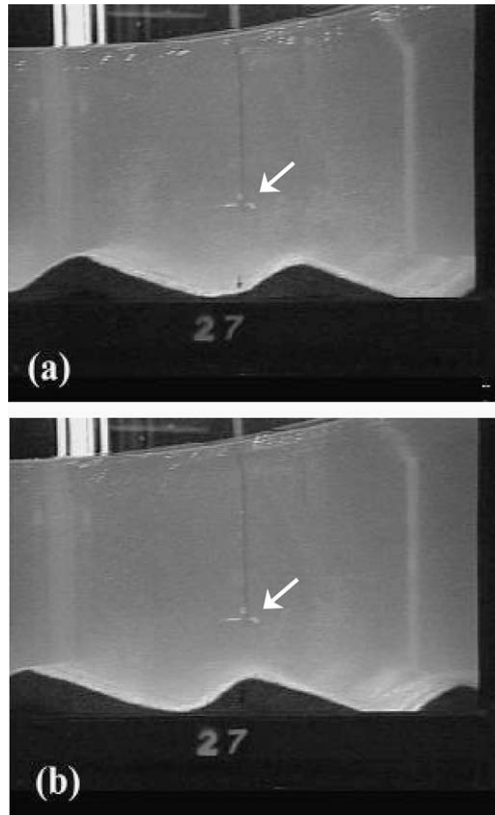


Fig. 12. Side view photograph (digitized image from video) showing the ADV probe above the drifting (from right to left) sand ripple. Experimental parameters: $\omega = 0.4$ Hz, $\epsilon_0 = 10$ cm, section 27. Frame (b) was taken 2.5 min after the frame (a). The ADV probe is barely visible and is shown by an arrow.

velocity over the measurement period was calculated as $U_d = 0.048 (\pm 0.007)$ cm s^{-1} . After collecting data on the ripple profile and drift, the ADV probe was rapidly traversed horizontally so that its measuring volume is at a location just above the ripple crest. Then the velocity measurements were taken while ripple drifted onshore.

Fig. 13 gives typical horizontal velocity traces. The data shown in Fig. 13a were taken approximately 5 cm above the ripple trough at the level of the ripple crest and the data shown in Fig. 13b were taken in the boundary layer approximately 0.1 cm above the ripple crest. The velocity magnitude at 5 cm above the trough is approximately twice that in the boundary layer above the crest. The averaged velocity over a wave period above the trough (Fig. 13a) is negative (offshore) while it is strongly positive just above the ripple crest (onshore) (Fig. 13b), pointing to the possibility of significant onshore sediment transport and hence a corresponding ripple drift.

The data in Fig. 13 present short pieces of a rather long (12 min) time record collected while the ripple drifted approximately a distance L_0 under the ADV probe. These data were time-averaged over five wave periods and the results are shown in

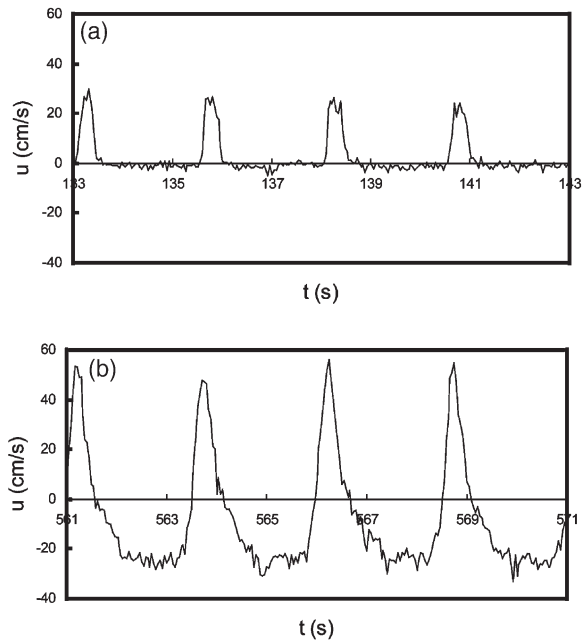


Fig. 13. Typical examples of horizontal along-slope velocity traces as obtained in the boundary layer approximately 0.1 cm above the ripple crest (a) and approximately 5 cm above the ripple trough at the level of ripple crest (b). The velocity magnitude at 5 cm above the trough (b) is approximately twice larger than in the boundary layer above the crest (a). As can be seen, averaged (over the wave period) velocity above the trough (b) is negative, while it is strongly positive just above the ripple crest (a). Time is given in accordance with Fig. 14 below. Experimental conditions are the same as in Fig. 11.

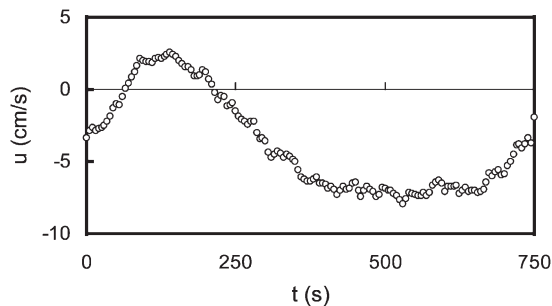


Fig. 14. Time record of the along-slope velocity component, u , averaged over five wave periods and taken at a level just above the ripple crest when the ripple slowly drifted one ripple length L_0 under the ADV probe. Experimental parameters are same as in Fig. 11.

Fig. 14. Note the positive mean water drift just above the ripple crest. This result is consistent with the measurements over solid ripples by Ridler and Sleath (2000) and justifies the use of (17) for estimating ripple drift velocity (18).

4. Evolution of sand bars

The type of breaker on a sloping beach depends on the beach slope and wave parameters. Battjes (1974) characterizes the waves by the surf similarity parameter

$$\xi = \tan\beta / \sqrt{\eta^* / \lambda}, \quad (19)$$

where β is the slope angle, η^* the wave amplitude near the break and λ the wavelength in deep water. Accordingly, a spilling breaker occurs when $\xi < 0.4$, a plunging breaker occurs when $0.4 < \xi < 2.0$ and a surging breaker occurs at larger ξ .

Depending on the range of parameters used in the experiments, spilling or plunging breakers can be generated, leading to different sandbar types; an example of a sandbar under a spilling breaker is shown in Fig. 15a, which has a bump-like shape. This case, even after breaking, waves are still energetic enough to form a large vortex onshore of the accumulated sand, causing offshore sediment motion and slow offshore drift of the bar. Note that this opposes the sediment transported by the onshore migrating ripples offshore of the bar.

In the case of a plunging breaker, sandbars of trapezoidal shape are formed. They have flat tops, small height and larger widths. Plunging breakers form closer to the shoreline and significant amount of energy is dissipated by a large vortex. The flow is not energetic enough to form another large vortex onshore side of the accumulated sand. Therefore, onshore mean sediment transport is observed and, as a result, bar slowly expands in the onshore direction.

5. Cobbles on a sandy slope

Literature on the behavior of cobbles on a sandy bed under progressive waves is virtually non-existent. Extending the work of Voropayev et al. (2001) that dealt with the solid slopes, we carried out a series of experiments to investigate this problem. The experiments were initiated with a flat sandy slope. Upon initiation of waves, ripples and bars are formed on the bed as was discussed above. When the system reached its quasi-steady state, cobbles were dropped on the bed and their behavior was monitored.

5.1. Cobble–ripple interaction

Consider the case where a relatively small and relatively light cobble (cobble D, E, F or G in Table 1) of size comparable to that of ripples is placed offshore of the break. At sufficiently large fluid velocities, the cobble moves onshore (Voropayev

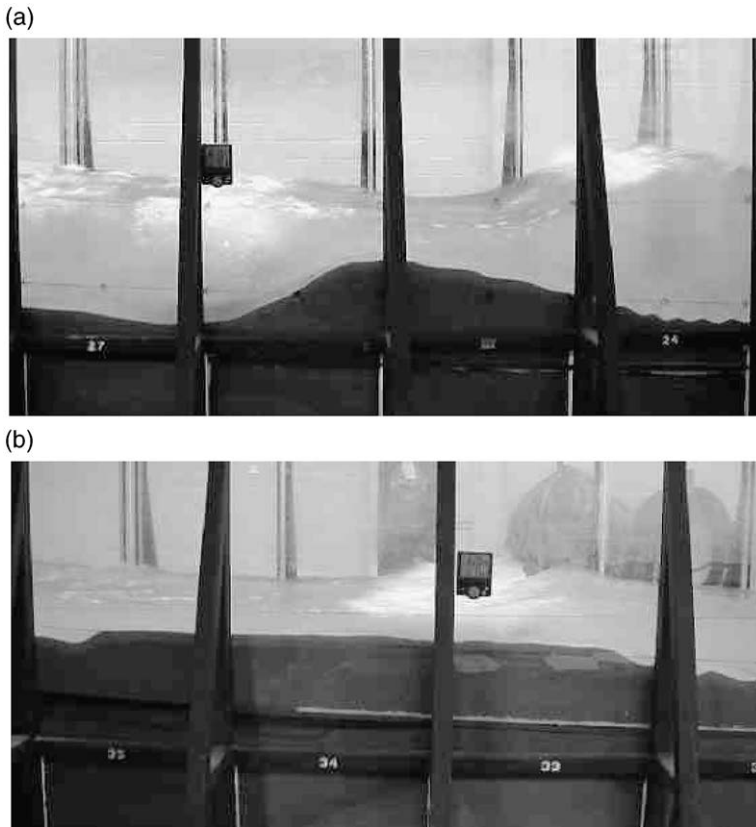


Fig. 15. Two typical examples of sandbars formed under spilling (a) or plunging (b) breakers. Experimental parameters: $\omega = 0.75$ Hz, $\epsilon_0 = 7.5$ cm (a), 0.6, 5 (b). Time is approximately $t = 140$ min (a), 75 (b) from the beginning of the experiment.

et al., 2001). The incoming waves pick up or tilt the cobble, facilitating it to slide or jump over the ripple located in front of it. Sometimes the cobble needs several attempts to pass over the nearby ripple. It is more difficult for a cobble to hurdle the ripples closer to the coastline as they are usually larger than ripples in deeper water, causing the cobble to entrap somewhere on its journey to the shore (Fig. 16a); the heavier the cobble, the easier it is trapped. When a cobble is trapped between two adjacent ripples, the flow field surrounding the cobble is changed considerably and becomes three-dimensional. Since the flow velocity surrounding the cobble increases relative to the background flow, scouring of the bed can be initiated. However, at relatively short times (1–2 h), the scouring appears to be of lesser importance (Voropayev et al., 1999) as compared to the ripple drift. Sediment from the ripple trough as well as from the ripple crest is transported towards the cobble, thus significantly changing the bottom topography close to the cobble and burying the cobble, at least partly, under migrating ripples (Fig. 16b). Cobble burial is a commonly

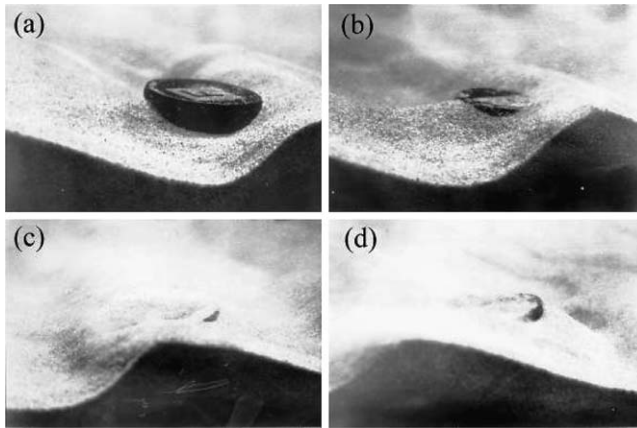


Fig. 16. Photographs showing the burial of a relatively small cobble that was trapped between two adjacent ripples. As can be seen ripples slowly drift from right to left. The trapped cobble (a) is first partly (b) and then completely (c) buried. In (d) it starts to recover again. Experimental parameters: $\omega = 0.4$ Hz, $\epsilon_0 = 12$ cm, section 27, cobble F (see Table 1). Time interval between frames (a) and (d) is approximately 6 min.

observed phenomenon when the cobble is trapped (see Fig. 16c,d). If the cobble and ripple sizes are comparable, the cobble can be buried completely and then unburied as the ripple above it drifts. This phenomenon leads to periodic burial of relatively small cobbles by drifting ripples. Typical period of such burial can be estimated as $T^* = L_0/U_d$, which is the time for a system of ripples to drift with a velocity U_d a distance equal to one ripple length L_0 . Estimating L_0 and U_d by using the formulas given in Section 3.2, one finds, for example, for conditions used in experiment shown in Fig. 18, $T^* = 6.5$ min, which shows a good agreement with the observations.

When larger cobbles (cobble 1, 2 or 3, see Table 1) of size larger than the ripple

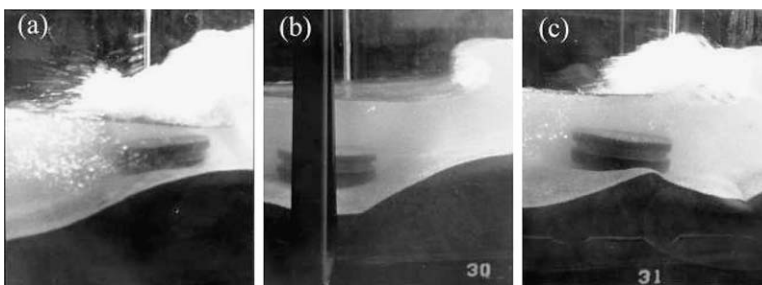


Fig. 17. Photographs showing the behavior of a large and relatively light cobble, which was initially above the sand bar when the incoming wave characteristics were changed. The cobble oscillates steadily above the bar in section 30 (a), then it slides to the trough at the onshore side of the bar (b) and finally moves steadily onshore in section 31 (c), reaching with time the shoreline (not shown). The initial bar in (a) was created under steady waves with $\omega = 0.75$ Hz, $\epsilon_0 = 6$ cm. Then in (b), (c) the wave intensity was reduced to $\epsilon_0 = 4$ cm. Cobble 2 was used in this run (see Table 1).

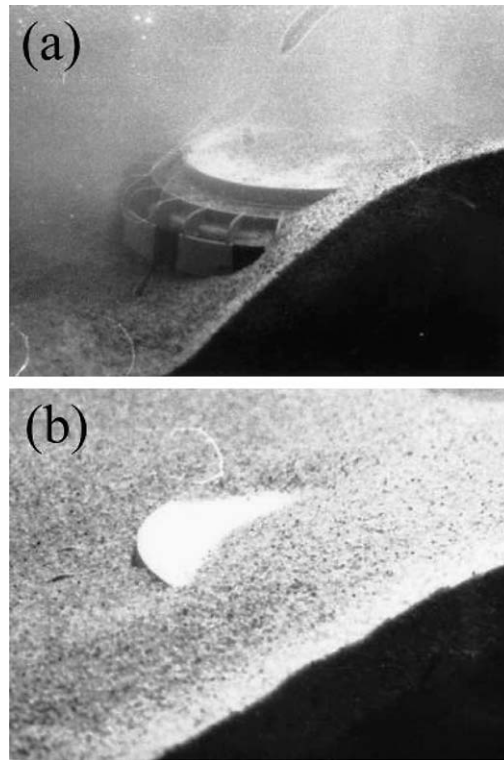


Fig. 18. Photographs showing the burial of a large and relatively heavy cobble, which initially was above the sand bar when the incoming wave characteristics were changed. The cobble (a) slides to the trough at the onshore side of the bar and is slowly buried (b) under the drifting bar. Experimental parameters are the same as in Fig. 16. Cobble 3 was used in this run.

height are introduced, they stay in one place (either stationary or oscillating back and forth about an equilibrium position) or slowly move onshore, depending on their density. With time, however, because of the local scour and ripple drift, the lower part of the cobble sank into the sand, immobilizing the cobble. The ripples drift slowly past the cobble, leading to partial periodical burial of the cobble.

If the cobble density is not sufficiently large, the cobble drifts onshore in small steps, oscillating back and forth around a slowly (shoreward) moving mean position. The asymmetry of driving forces (waves) appears to be responsible for this migration (Voropayev et al., 2001). Usually, during the onshore displacement, the cobble is detached from the bottom (see e.g., Fig. 13 in Voropayev et al., 2001), while the offshore movement is associated with the cobbles sliding along the bed. During their onshore motion, larger cobbles do not follow the ripple movement, but they plough (bulldoze!) through ripple crests and arrive in shallower water where sand bars are usually formed.

5.2. Cobble–bar interaction

As mentioned, at large times a sand bar of size much larger than the cobble is established under the breaking waves (see Fig. 17). The water depth decreases rapidly along the slope of the bar, and hence the flow becomes more energetic and provides enough momentum for the cobbles to climb along the sloping bar and reach its top.

If the incoming wave characteristics remain fixed, a quasi-equilibrium state can be established during which the cobbles stay near the top of the bar for a period of time (0.5 h or more); they, however, oscillate back and forth under the wave action (Fig. 17a). This observation can be explained as follows. The onshore water motion above the bar is very energetic and forces the cobble onshore. In addition, the incoming waves break here and a large vortex is formed under the wave crest, resulting in an intense turbulent bore that propagates onshore (swash flow). Return flow in the swash is less energetic, yet sufficiently strong and propagates near the bottom under the bore. The returning swash flow and the offshore motion (generated under the wave trough) cause the cobble to move offshore, following its onshore motion. The oscillations of the cobbles at the top of the bar occur by these two competing mechanisms. This position, however, may not be stable. Due to intense turbulent motion, the cobble may tip and slide down along the bar. When the cobble slides to the offshore side of the bar, it is usually pushed back to the top of the bar and start oscillating again. If it slides along the onshore side of the bar, the cobble can either be pushed back to the top of the bar or get entrapped there.

Changing of incoming wave characteristics alters the position of the break point and hence the behavior of cobbles. The associated processes are intricate, and here we present an example to illustrate this complexity. When the paddle oscillations are changed to a lower frequency or smaller amplitude, the waves break closer to the coastline and the bar drifts onshore. Thence, the back flow above the bar is significantly reduced and the cobble slides down from the bar crest along the onshore side (Fig. 17b). The general behavior of cobble depends on the cobble density. If the cobble is relatively light, it moves slowly onshore, reaches the swash region and (usually) continues to move (Fig. 17c) under the turbulent bore until it arrives at the shoreline. If the cobble is relatively heavy, it tends to be trapped in the onshore face of the bar. Because of the slow onshore migration of the bar, the cobble can be completely buried under the bar, as shown in Fig. 18, for a long period of time. This burial process is rather slow and can take several hours.

6. Conclusions

The evolution of an initially flat sandy slope and the behavior of disk-shaped objects placed therein under shoaling progressive waves were studied experimentally. This problem is closely related to the drift and scour/burial of objects, such as cobbles/mines, in the shoaling region of a surf zone. The experiments were conducted in a large wave tank with a sandy slope. Upon initiation of wave forcing, the initially flat topography changes and after a transitional time, the bedform reaches a quasi-

steady state with a system of sand ripples and a large bar near the break. Although the incoming wave characteristics are fixed, the bottom topography never reaches a full steady state but evolves slowly (e.g. ripple drift and sandbar transformation at large times). The data on the ripple formation, growth, drift, and quasi-steady ripple characteristics were collected and compared with simplified theoretical predictions. When the incoming wave characteristics were changed, the bottom topography responded by establishing a new quasi-steady state after a certain adjustment time period.

Data on wave-induced flow characteristics in the vicinity of the movable bed were obtained using acoustic Doppler velocimetry. The presence of a mean onshore flow in the boundary layer above the ripple crest was observed, corroborating the observations of Ridler and Sleath (2000) carried out in the wave boundary layer above a solid sinusoidal bedform.

The above studies were extended to include model cobbles/mines of different sizes and densities placed along the sandy slope. Four different scenarios were identified: (i) steady oscillations of cobbles with zero mean displacement and small scour; (ii) mean onshore motion of relatively light cobbles, (iii) periodic burial of relatively heavy cobbles of which the dimensions are comparable to that of sand ripples, (iv) burial of relatively large cobbles under the bar when the break point was changed by changing incoming wave characteristics. Physical explanations were provided to explain the observations.

Acknowledgements

This study was supported by the Office of Naval Research, Grants N00014-95-1-0543 and N00014-01-1-0349. We are grateful to Marcel Creamers for helping in the experiments.

References

- Andersen, K.H., 2001. A particle model of rolling grain ripples under waves. *Phys Fluids* 13 (1), 58–64.
- Arcilla, A.S., Stive, M.J.F., Kraus, N.C. (Eds.), 1994. *Coastal Dynamics '94*. Amer. Society of Civil Eng., New York.
- Battjes, J.A., 1974. Surf similarity. In: *Proc. 14th Coastal Eng. Conf.*, American Society of Civil Engineering, New York, pp. 466–480.
- Battjes, J.A., 1988. Surf-zone dynamics. *Ann. Rev. Fluid Mech* 20, 257–293.
- Belorgey, M., Rajaana, R.D., Sleath, J.F.A. (Eds.), 1993. *Sediment Transport Mechanisms in Coastal Environments and Rivers*. World Scientific, Singapore.
- Blondeaux, P., 1990. Sand ripples under sea waves. Part 1. Ripple formation. *J. Fluid Mech.* 218, 1–17.
- Blondeaux, P., Foti, E., Vittory, G., 2000. Migrating sea ripples. *Eur. J. Mech. B-Fluids* 19, 285–301.
- Craik, A.D.D., 1985. *Waves Interactions and Fluid Flow*. Cambridge University Press, Cambridge.
- Dean, R.G., Dalrymple, R.A., 1994. *Water Wave Mechanics for Engineers and Scientists*. World Scientific, Singapore.
- Elfink, B., Baldock, T., 2002. Hydrodynamics and sediment transport in the swash zone: A review and perspectives. *Coastal Eng* 45, 149–167.

- Engelung, F., 1970. Instability of erodible beds. *J. Fluid Mech.* 42, 225–244.
- Engelund, F., Fredsøe, J., 1982. Sediment ripples and dunes. *Ann. Rev. Fluid Mech* 14, 13–37.
- Fredsøe, J., Deigaard, R., 1992. *Mechanics of Coastal Sediment Transport*. Advanced Series on Ocean Engineering, 3. World Scientific, Singapore.
- Grilli, S.T., Horillo, J., 1997. Numerical generation and absorption of fully nonlinear periodic waves. *Journal of Engineering Mechanics* 123 (10), 1060–1069.
- Grilli, S.T., Svendsen, I.A., Subramanya, R., 1997. Breaking criterion and characteristics for solitary waves on slopes. *J. Waterw., Port, Coastal Ocean Engr* 123 (3), 102–112.
- Grilli, S.T., Voropayev, S.I., Testik, F.Y., Fernando, H.J.S. 2003. Numerical and experiments of wave shoaling over semi-buried cylinders in sandy bottom. In: *Proceedings of the 13th International Offshore and Polar Engineering Conference*, Honolulu, accepted for publication.
- Horikawa, K., Wanatabe, A., 1967. A study of sand movement due to wave action. *Coastal Engng Japan* 10, 39–57.
- Kennedy, J.F., 1963. The mechanics of dunes and antidunes in erodible-bed chanals. *J. Fluid Mech.* 16, 521–544.
- Longuet-Higgins, M.S., Stewart, R.W., 1964. Radiation stress in water waves; a physical discussion with applications. *Deep Sea Res* 11, 529–562.
- Luccio, P.A., Voropayev, S.I., Fernando, H.J.S., Boyer, D.L., Houston, W.N., 1998. Motion of cobbles in the swash zone on an impermeable slope. *Coastal Eng* 33, 41–60.
- Mei, C.C., 1982. *The Applied Dynamics of Ocean Surface Waves*. John Wiley and Sons, New York.
- Mei, C.C., Liu, P.L., 1993. Surface waves and coastal dynamics. *Ann. Rev. Fluid Mech* 25, 215–240.
- Mei, C.C., Yu, J., 1997. Note on the instability of sand ripples under partially standing surface waves. *Phys. Fluids* 9, 1606–1620.
- Nielsen, P., 1992. *Coastal Bottom Boundary Layer and Sediment Transport*. World Scientific, London.
- Peregrine, D.H., 1983. Breaking waves on beaches. *Ann. Rev. Fluid Mech* 15, 149–173.
- Ridler, E.L., Sleath, J.F.A., 2000. Effect of bed roughness on time-mean drift induced by waves. *J. Waterway, Port, Coastal and Ocean Div., ASCE* 126 (1), 23–29.
- Sleath, J.F.A., 1976. On rolling grain ripples. *J. Hydraul. Res.* 14, 69–81.
- Sleath, J.F.A., 1984. *Sea Bed Mechanics*. John Wiley and Sons, New York.
- Sleath, J.F.A., 1995. Sediment transport by waves and currents. *J. Geophys. Res* 100 (C6), 1097–1098.
- Snyder, W.H., Castro, P.I., 1999. Acoustic-Doppler-velocimeter evaluation in a stratified tank. *J. Hydraulic Eng., ASCE* 125 (6), 595–603.
- Vittory, G., Blondeaux, P., 1990. Sand ripples under sea waves. Part 2. Finite-amplitude development. *J. Fluid Mech.* 218, 19–39.
- Voropayev, S.I., Roney, J., Fernando, H.J.S., Boyer, D.L., Houston, W.N., 1998. The motion of large bottom particles (cobbles) in a wave-induced oscillatory flow. *Coastal Eng* 34, 197–219.
- Voropayev, S.I., McEachern, G.B., Boyer, D.L., Fernando, H.J.S., 1999. Dynamics of sand ripples and burial/scouring of cobbles in oscillatory flow. *Applied Ocean Res* 21 (5), 249–261.
- Voropayev, S.I., Cense, A.W., McEachern, G.B., Boyer, D.L., Fernando, H.J.S., 2001. Dynamics of cobbles in the shoaling region of a surf zone. *Ocean Eng* 28 (7), 763–788.
- Voropayev, S.I., Testik, F.Y., Fernando, H.J.S., Boyer, D.L., 2003. Burial and scour around a short cylinder under progressive shoaling waves. *Ocean Eng.*, accepted for publication.
- Yalin, M.S., 1977. *Mechanics of Sea Bed Transport*. Pergamon, New York.